Carbon 98 (2016) 449–456

Contents lists available at ScienceDirect

Carbon

journal homepage: www.elsevier.com/locate/carbon

Covalent pathways in engineering *h*-BN supported graphene

Bin Ouyang, Jun Song*

Department of Mining and Materials Engineering, McGill University, 3610 University Street, Montreal, QC, H3A 0C5, Canada

ARTICLE INFO

Article history:
Received 4 June 2015
Received in revised form
28 September 2015
Accepted 27 October 2015
Available online 7 November 2015

ABSTRACT

Cross-planar di-vacancies (CPDVs) within stacked graphene hexagonal boron nitride (*h*-BN) heterostructures provide stabilized covalent links to bridge adjacent graphene and *h*-BN sheets. Through a first principle theoretical study based on density functional theory (DFT), it was shown that the CPDVs serve as focal points for cross-planar atom diffusion between graphene and *h*-BN, and the chemical nature of interlayer links along with associated cross-planar migration pathways at these defects can be predictively manipulated through modulation of the chemical environment and charge engineering, to achieve consistent B or N doping and simultaneous healing of graphene. The present study proposed a viable approach integrating irradiation, chemical and charge engineering, to produce high-quality graphene with tunable electronic and electrochemical properties, using the *h*-BN substrate.

1. Introduction

Interface coupling between graphene and its insulating isomorph, hexagonal boron nitride (*h*-BN) provides interesting possibilities for the synthesis and engineering of graphene-based two-dimensional nanomaterials. The predominant Van der Waals interactions between them enables an atomic sharp interface that minimizes dangling bonds and charge traps, making *h*-BN as a promising substrate for high-quality graphene devices. Meanwhile the accompanying electronic coupling between graphene and *h*-BN leads to compelling physical phenomena, such as breakage of time reversible symmetry [1–4], commensurate to incommensurate transition [5–7], and Hofstadter butterfly [4,8,9], promising numerous ways to manipulate graphene devices through periodic potential.

Besides the above coupling effects derived from the long-range dispersive interlayer interactions, the interplay between graphene and *h*-BN may also be affected by discrete covalent connections. Telling et al. [10] demonstrated the existence and ground states of cross-planar di-vacancies (CPDVs), namely Wigner defects in graphite. These defects, introduced via high-energy (e.g., irradiation) and high-temperature processes [11–13], induce local three-dimensional (3D) reconstruction and bridges adjacent atomic sheets in graphite through covalent bonds. Given the close structural resemblance between graphene and *h*-BN, and sp2 hybridization bonding in both materials, CPDVs are also expected to exist at the graphene/*h*-BN interface. These defects have great implications for the *h*-BN supported graphene. Aside from the well expected strengthening attributed to the interlayer covalent bonding as hinted in previous studies on graphite and carbon nanotubes (CNTs) [12,14–16], the CPDVs create stabilized links between graphene and the two non-equivalent sublattices in *h*-BN. These links (i.e., C–B or C–N) are of distinct energy states, bond polarization and electronic structures, and can act as potential focal points for structural evolution and electron doping of graphene. In this paper, we present the first systematic study of CPDVs at the graphene/*h*-BN interface, and show that those CPDVs can provide effective pathways for cross-planar atom diffusion. Moreover, through modulation of the chemical environment and charge state, the cross-planar diffusion can be manipulated to yield controlled B or N doping of graphene. Simultaneously with the doping of graphene, the CPDV converts to an in-plane di-vacancy (DV) in *h*-BN and the cross-planar covalent bond gets annihilated, resulting in healing of vacancies in graphene. These findings promise viable routes to manipulate defect evolution to enable compositional and electrochemical engineering of *h*-BN supported graphene.

2. Computational methodology

Stacked bilayer graphene/h-BN heterostructures consisting of one layer of graphene and h-BN each are considered in the present study. In our simulations, an 8 × 8 of unit cell is used. The simulation cell is shown to be large enough to eliminate interactions

* Corresponding author.
E-mail address: jun.song2@mcgill.ca (J. Song).

http://dx.doi.org/10.1016/j.carbon.2015.10.100
0008-6223/

between defects and their periodic images. The lattice constants of graphene and h-BN are set to be the same, being $a_0 = 2.49$ Å which is found to yield the lowest total energy. The dimension of the vacuum space perpendicular to the bilayer heterostructure is set as 15 Å to avoid image interaction [17]. There are three possible stable stacking configurations for bilayer graphene/*h*-BN stacking with slight stacking energy difference. In this paper, the stacking with N atom on top of the hexagonal center of graphene (AB-GBN) is selected as it represents the most stable stacking configuration [18]. Lattice defects are then introduced into the bilayer structures to construct different defect complexes.

Spin polarized DFT calculations were performed using the Vienna ab-initio Simulation Package (VASP) [19] with projector augmented-wave (PAW) [20–24] pseudopotentials. A cutoff energy of the plane wave basis set of 500 eV is used in all calculations. Further increase in the cutoff energy up to 800 eV will only introduce a tiny energy difference <0.02 eV. The climbed image Nudged Elastic Band (ci-NEB) method is employed to calculate minimum reaction paths (MEPs) of migration processes [25–28]. The D2 method of Grimme is adopted to consider the weak Van der Waals interactions [29]. A 3 × 3 Gamma centered *k*-point grid is used in all calculations [30]. Both the structure optimization and ci-NEB calculations are regarded converged when the force per atom is < 0.01 eV/Å.

3. Results and discussions

3.1. The ground states and electronic structures for CPDVs

A CPDV at the graphene/*h*-BN interface is formed when two single vacancies (SVs) at adjacent sheets coalesce. For the coalescence to occur, the two SVs need to be in close vicinity of each other to enable the overlap of cross-planar dangling orbitals so that bond reconstruction can be induced by lattice fluctuation. Fig. 1 shows the eight possible CPDV configurations (immediately before the coalescence of SVs) at the graphene/*h*-BN interface, identified via DFT calculations.

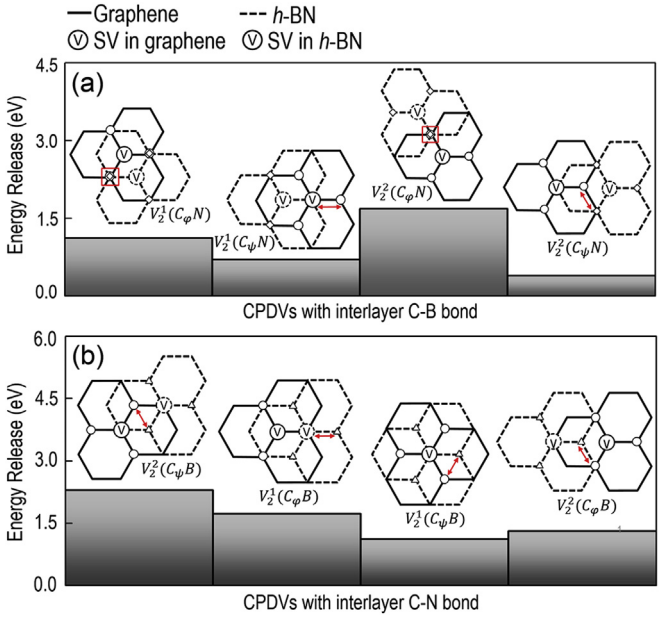

Fig. 1. The corresponding energy release associated with the formation of CPDVs with (a) interlayer C–B links and (b) interlayer C–N links. The insert figures illustrate the local configurations of corresponding SV couples prior to the CPDV formation. The atom pairs responsible for the interlayer links are indicated by red squares or left-right arrows. Dangling C, B and N atoms neighboring CPDVs are indicated by open circles, open diamonds and open triangles respectively (A colour version of this figure can be viewed online).

For simplicity, we adopt a notation similar to what Telling et al. used in Ref. [10] to distinguish different CPDV complexes. As illustrated in Fig. 1, a CPDV configuration is denoted as $V_2^i(C_\alpha X)$ where the superscript $i = 1$ or 2 indicate that the constituent vacant sites are 1st or 2nd nearest interplanar neighbors with each other, C_α refers to the missing C atom of which α represents two sublattices in graphene layer that could be either ψ (sublattice sits on top of B atom) and φ (sublattice sits on top of the hexagon center of *h*-BN), and *X* stands for the missing atom in *h*-BN (either B or N atom). The constituent single vacancies are denoted as SV_C, SV_B and SV_N, referring to the single C vacancy in graphene, and single B and N vacancies in *h*-BN respectively.

The ground states of those CPDVs are obtained through structural optimization in DFT calculations. The coalescence from two interlayer SVs into a CPDV leads to sizable energy release, clearly noted in Fig. 1. Fig. 2a and b shows the relaxed atomic configurations of two representative CPDVs with C–B covalent bonds, i.e., $V_2^1(C_\psi N)$ and $V_2^2(C_\psi N)$ where graphene and *h*-BN sheets are bridged by interlayer C–B bonds. We can note that in both cases the interlayer bond induces considerable basal shearing and local buckling at the CPDV. Particularly for $V_2^1(C_\psi N)$, the interlayer bond produces a basal shift of 0.17 Å along the armchair (AC) direction, and displaces the C and B atoms away from their corresponding host atomic sheets by 0.65 Å and 1.24 Å respectively (cf. Fig. 2a), while for $V_2^2(C_\psi N)$, the interlayer bond results in a basal shift of 0.38 Å along the zigzag (ZZ) direction, and displaces the C and B atoms away from their corresponding host atomic sheets by 0.79 Å and 0.94 Å (cf. Fig. 2b). Similar phenomena are also observed for CPDVs with interlayer C–N bonds, also illustrated by the two representative cases, i.e., $V_2^1(C_\varphi B)$ with displacements of C and N atoms being respectively 1.00 Å and 1.01 Å and a basal shift of 0.19 Å along AC direction, and $V_2^2(C_\varphi B)$ with displacements of C and N atoms being respectively 0.89 Å and 1.11 Å and a basal shift of 0.51 Å, shown in Fig. 2c and d respectively. These distortions are identified to be of direct relevance in determining the energetics of CPDVs (see Supplementary Material).

With the large local geometry modification, the CPDV necessarily induces significant perturbation in the spatial partial charge distribution. From the electronic structures deduced from DFT calculations, the Scanning Tunneling Microscope (STM) [31,32] images of the aforementioned CPDVs are simulated, shown alongside with the corresponding atomic configurations in Fig. 2. We can see that CPDVs induce significant contrast in those simulated STM images. Meanwhile we can also note that the contrast is strongly correlated with the local geometrical characteristics associated with the CPDV, suggesting that CPDVs can be readily identified and distinguished in experiments employing STM.

3.2. Atom diffusion across graphene/h-BN interface through CPDVs

Locally at a CPDV, the adjacent graphene and *h*-BN sheets are distorted towards each other. In particular, the two atoms (i.e., C and B or C and N) that constitute the interlayer links are considerably displaced towards the opposite layers. These features would presumably aid cross-planar kinetics. In this regard, we systematically examined the cross-planar migration pathways at CPDVs combing DFT with transition state theory (TST) [25–28]. In our discussion below, $V_2^1(C_\psi N)$ and $V_2^1(C_\varphi B)$ are selected to represent CPDVs with interlayer C–B and C–N bonds respectively. The possible cross-planar migration scenarios and associated minimum

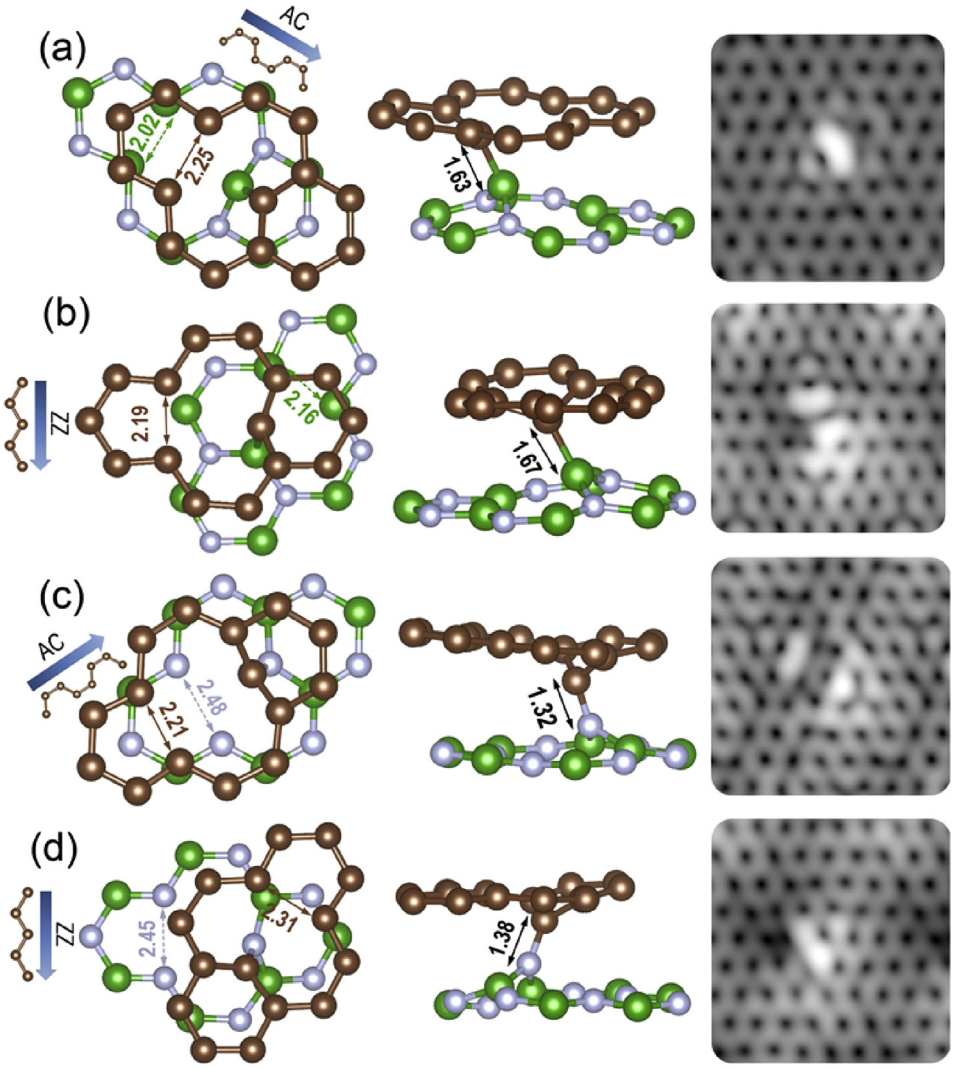

Fig. 2. The top and side views of the ground-state configurations of several representative CPDVs: (a)$\boldsymbol{V}_2^1(\boldsymbol{C}_\psi\boldsymbol{N})$, (b) $\boldsymbol{V}_2^2(\boldsymbol{C}_\psi\boldsymbol{N})$, (c) $\boldsymbol{V}_2^1(\boldsymbol{C}_\varphi\boldsymbol{B})$ and (d) $\boldsymbol{V}_2^2(\boldsymbol{C}_\varphi\boldsymbol{B})$. The subfigures in the rightmost column are the simulated STM images of those CPDVs. In the STM simulation, the partial charge range from E_F-1.5 eV to E_F (with E_F being the corresponding Fermi energy) is considered to capture the defective charge state. C, B and N atoms are colored dark brown, green and silver respectively (A colour version of this figure can be viewed online).

energy paths (MEPs) at $V_2^1(C_\psi N)$ and $V_2^1(C_\varphi B)$ are shown in Fig. 3. There are two possible routes for cross-planar migration at a CPDV with the interlayer C-X (X = B or N) bond, i.e., A) atom diffusion towards graphene, resulting in X-doping of graphene and a planar divacancy in h-BN (DV_{BN}), or B) atom diffusion towards h-BN, resulting in C-doping of h-BN and a planar divacancy in graphene (DV_C), both yielding further energy release compared to the CPDV. In particular for $V_2^1(C_\psi N)$, the migration route A exhibits an energy barrier of 0.76 eV and results in an energy release of 1.43 eV with respect to $V_2^1(C_\psi N)$, while the migration route B shows a much higher energy barrier of 2.79 eV and leads to a smaller energy release of 0.75 eV. Meanwhile for $V_2^1(C_\varphi B)$, the migration route B is both kinetically and energetically favored over route A, showing a lower energy barrier of 0.98 eV (than 1.57 eV in route A) and higher energy release of 4.84 eV (than 3.83 eV in route A). One thing to note is that cross-planar migration at a CPDV always results in energy release and is thus thermodynamically favored. The energy release is well expected by looking at the formation energy of the post-migration defect complex (denoted as E_f^{PM} below), which can be roughly estimated from individual energetics data of defects in graphene and h-BN systems [33–40],

$$E_f^{PM} \approx \begin{cases} E_f[DV_{BN}] + E_f[C_X], & \textit{Route A} \\ E_f[DV_C] + E_f[X_C], & \textit{Route B} \end{cases} \quad (1)$$

where $E_f[DV_{BN}]$ and $E_f[DV_C]$ denote the formation energies of a divacancy in h-BN and graphene respectively, $E_f[C_X]$ denotes the formation energy of a substitutional impurity X (X = B or N) in graphene, and $E_f[X_C]$ denotes the formation energy of a C impurity that substitutes X atom in h-BN. Besides the above migration routes, we also examined the possibility of simultaneous diffusion of neighboring B and N. However this dual-atom diffusion exhibits significantly higher energy barrier (see Supplementary Material for details). Therefore it is expected to be a rare event under normal circumstances and not considered in our discussion below.

Among the various cross-planar migration possibilities at a CPDV, of particular interest are the ones that lead to atom (B or N) diffusion towards graphene. As illustrated in Fig. 3, they result in B or N doping of graphene, which consequently can modify the electronic, chemical and magnetic properties as well as electrocatalytic activity of graphene [30,34,41–44]. In addition, those dopants fill in the otherwise vacant sites in graphene to help improve the lattice quality. This essentially leads to *healing* of

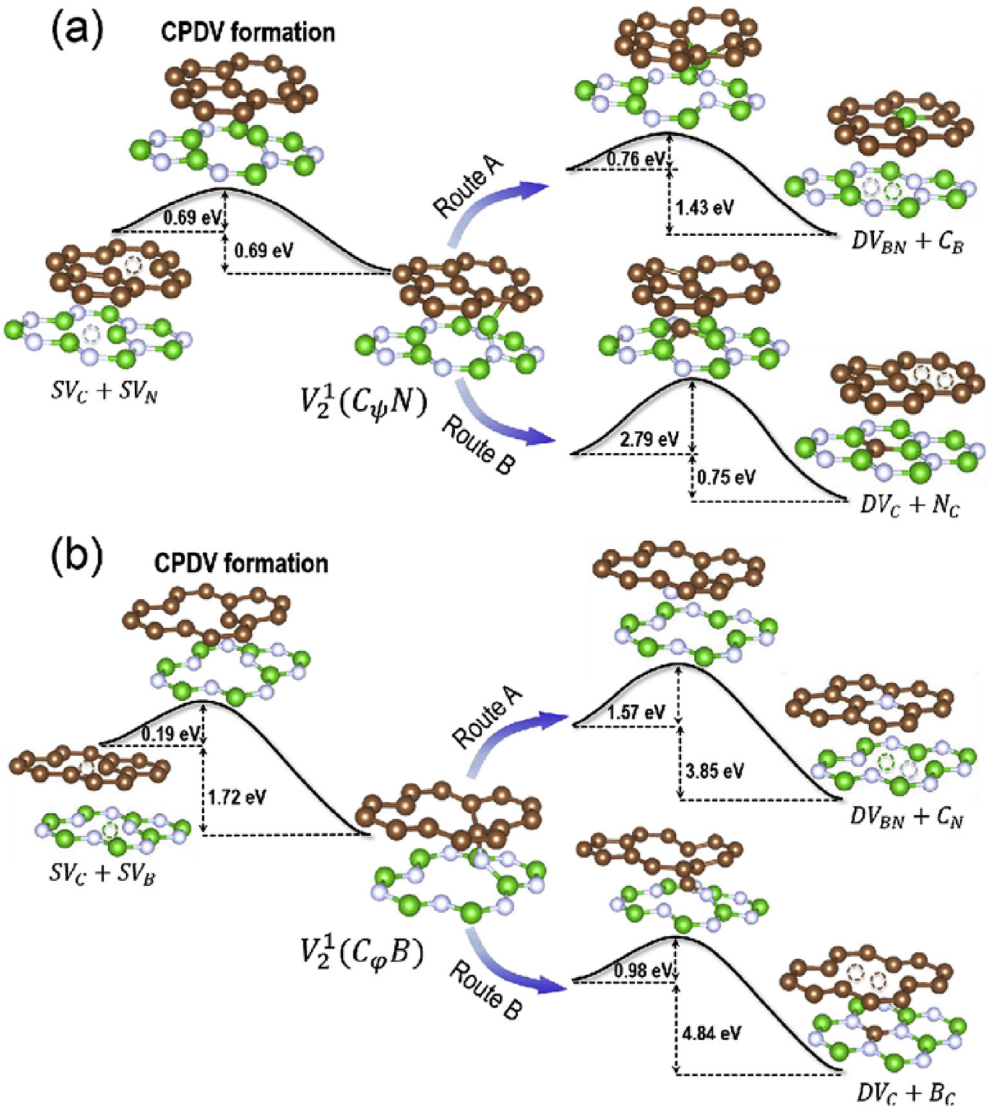

Fig. 3. The kinetics and reaction pathways of defect formation and subsequent cross-planar migration at two representative CPDVs: (*a*) $\mathbf{V}_2^1(\mathbf{C}_\psi\mathbf{N})$ and (*b*) $\mathbf{V}_2^1(\mathbf{C}_\varphi\mathbf{B})$, with the corresponding migration barriers indicated. C, B and N atoms are colored dark brown, green and silver respectively. The dashed circles indicate the SVs (SV_C: brown; SV_B: green and SV_N: silver) prior to the CPDV formation and divacancies (i.e., represented as SV couples) post migration (A colour version of this figure can be viewed online).

graphene lattice, hinting a strategy to moderate defect density during doping of graphene. Nonetheless, these migration paths will be competing with the ones that result in atom diffusion towards *h*-BN which in sharp contrast further deteriorate the quality of the graphene. For instance, in the case of $V_2^1(C_\varphi B)$, the C doping of *h*-BN (i.e., route B) is both thermodynamically and kinetically favored over the N doping of graphene (i.e., route A). The above competition provides an interesting implication (and challenge) on the synthesis of impurity (i.e., B or N) doped graphene with enhanced lattice quality. To put things into context, below we discuss the formation of CPDVs and migration at CPDVs in possible experimental settings.

3.3. Manipulating defect structure evolution through charge and chemical potential

One method often adopted in experiments to induce cross-planar defects in carbon-based nanomaterials is electron [45–47] or ion irradiation [48,49]. The irradiation approach has been widely used to modify the structural properties of, e.g., CNTs [11,12,14,15,47–49], graphite [10,16,35] and other 2D structures [33,50–52]. During irradiation, the incoming particles deploy sufficient energy to cause large out-of-plane displacements of atoms and thus aid the formation of covalent interlayer links. With the graphene/*h*-BN system being structurally similar to CNTs and graphite, one can imagine that the irradiation method can also serve as an effective means to generate CPDVs between graphene and *h*-BN sheets. The different flavor is, however, that we would expect two different sets of interlayer links, C–B and C–N, rather than the C–C links in those pure carbon-based systems previously studied [10,12,13,15,16]. Consequently the formation along with the bonding characteristics of the interlayer link of a CPDV in the graphene/*h*-BN system depend on the chemical environment (i.e., B-rich or N-rich) of the experiment. This dependence of chemical environment apparently also applies to those defect complexes that derive from CPDVs (e.g., the post-migration systems, cf. Eq. (1)). Another important aspect of electron or ion irradiation is that it naturally brings charge into the material system treated [33,35,53,54]. This modifies the charge state of the material system and introduces another dimension of influence to tune the

energetics of resultant defect complexes. Accounting for the effects of chemical environment and charge state, we can formulate the formation energy, E_f^q, of a defect in the graphene/*h*-BN heterostructure as [35,36,55,56]:

$$E_f^q = E_{\text{tot}}^q - N_B\mu_B - N_N\mu_N - N_C\mu_C - qE_F^q \quad (2)$$

where q denotes the charge state of the system, E_f^q and E_F^q denote the total energy and Fermi energy of the system with a charge state q, N_C, N_B and N_N are the numbers of C, B and N atoms respectively, and μ_C, μ_B and μ_N are the chemical potentials of C, B and N elements respectively.

Using Eq. (2) and assuming the dilute limit of defects, the formation energies of CPDVs and associated defect complexes are examined. Considering a scenario where CPDVs are introduced into the graphene/*h*-BN system through irradiation, we outline the evolution possibilities of the system in Fig. 4a, where depending on the resultant defect complex of the lowest formation energy the 2D phase space of chemical environment and charge state is partitioned into different domains. Several key observations can be drawn from Fig. 4a. Firstly we note that in general the graphene/*h*-BN with CPDVs will always undergo the cross-planar migration process to transform into impurity doped graphene plus DV decorated *h*-BN (i.e., $C_X + DV_{BN}$ with X = B or N) or C doped *h*-BN plus DV decorated graphene (i.e., $X_C + DV_C$ with X = B or N). The resultant concentration of doping is shown to directly depend on the concentration of CPDVs (see Supplementary Material for details), which can be tuned by adjusting chemical potential, charge state and irradiation energy intensity. Secondly we see that the defect complexes in the left three domains (i.e., light purple and yellow domains) where the environment is largely B-rich derive from CPDVs with interlayer C—B links while those defect complexes in the right two domain where the environment is largely N-rich derive from CPDVs with interlayer C—N links, suggesting that the bonding nature at a CPDV can be controlled by varying the chemical potential of B or N. In addition, we see that the cross-planar migration route at a CPDV can be precisely regulated via the charge state. This is of particular significance as it enables unidirectional atom diffusion from *h*-BN to graphene to grant consistent doping and healing of graphene. Fig. 4a provides a predictive mapping of structural evolution for irradiated graphene/*h*-BN heterostructures, and suggests a novel approach, integrating irradiation, modulation of chemical potential and charge engineering to predictively functionalize graphene on top of *h*-BN, as schematically illustrated in Fig. 4b. The inserted subfigure (enclosed in a dashed oval) in Fig. 4b shows a schematic setup of electron gating, one feasible route to realize charge engineering in experiments. Based on the previous study by Efetov and Kim [57], sizable charging doping can be achieved (see Supplementary Material for details).

There are however a couple of things to note for the predictive mapping shown in Fig. 4a, particularly when interpreting its

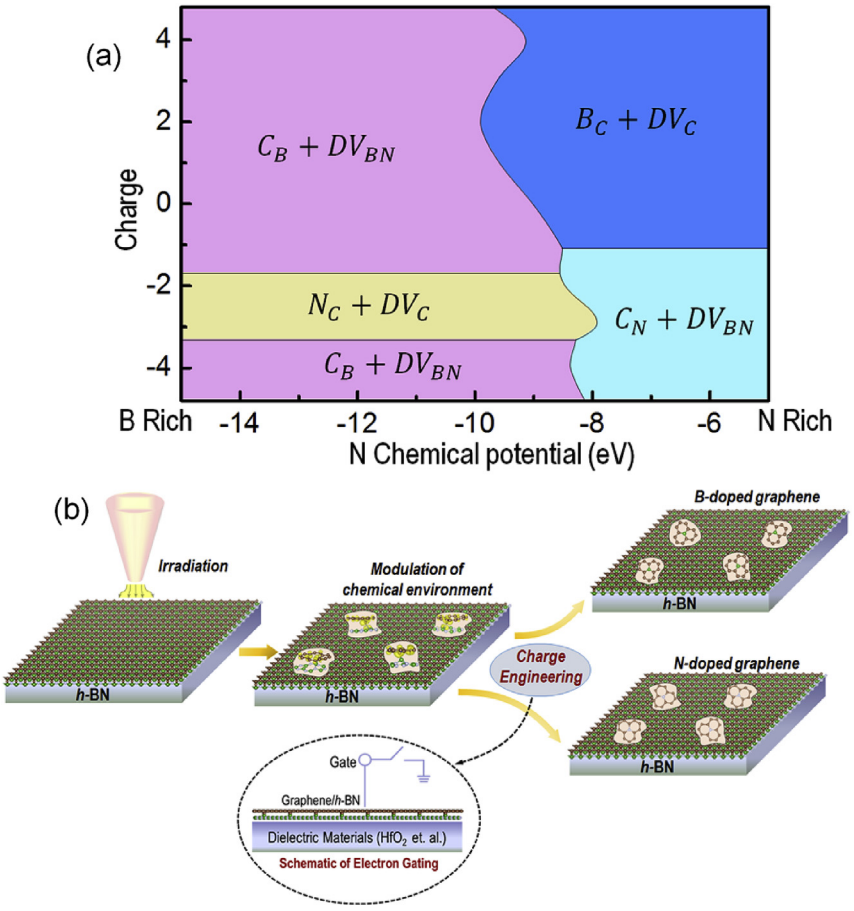

Fig. 4. (*a*) Predictive mapping of the evolution possibilities of irradiated stacked graphene/*h-BN* heterostructures as the chemical potential and charged state vary; (b) Schematic illustration of the possible experimental procedure to use electron or ion beam irritation to induce CPDVs in *h*-BN supported graphene, augmented by chemical potential and charge engineering to achieve controlled B or N doping of the graphene sheet. The subfigure enclosed in dashed oval illustrates the route of electron gating to achieve charge doping in experiments (A colour version of this figure can be viewed online).

implications to experimental fabrication. First, Fig. 4a is derived on a thermodynamic basis, while in reality the structural evolution can be greatly affected by kinetics as well. To this end, additional calculations have been performed to assess how the mapping would be modified in the presence of kinetics. Our preliminary results show that kinetics can blur the boundaries between those domains in the mapping, leading to regimes where different structural possibilities co-exist. Nonetheless the essential trends of structural evolution remain well captured by Fig. 4a (see Supplementary Material for details). Second, besides the chemical potential and charge state, the mapping may also be influenced by the presence of lattice defects, e.g., SVs. For instance, the formation of $V_2^1(C_\varphi B)$ and will be favored in a graphene/*h*-BN system rich in SV_B s while the formation of $V_2^1(C_\psi N)$ will be favored in a graphene/*h*-BN system rich in SV_N s, which in effect will shift the mapping towards *B*-rich and *N*-rich sides respectively. Additionally, SVs in a graphene/*h*-BN system may interact with CPDVs to form stable extended defect complexes, thereby inhibiting further structural evolution at CPDVs (see Supplementary Material for details).

To understand the pronounced effects of charge on structural evolution at CPDVs, we examine the formation energetics and electronic structures of charge doped CPDVs and their associated defect complexes. Fig. 5 shows the formation energy difference (ΔE_f^q) and Fermi energy difference (ΔE_F^q) of different structural evolution possibilities at two representative CPDVs, i.e., $V_2^1(C_\psi N)$ in a B-rich environment [58] and $V_2^1(C_\varphi B)$ in a N-rich environment [59], as the charge state q varies, with

$$\Delta E_f^q = E_f^q[\mathrm{TS}] - E_f^q\left[V_2^i(C_\alpha X)\right], \tag{3}$$

$$\Delta E_F^q = E_F^q[\mathrm{TS}] - E_F^q\left[V_2^i(C_\alpha X)\right], \tag{4}$$

where $E_f^q[\mathrm{TS}]$ and $E_F^q[\mathrm{TS}]$ respectively denote the formation energy and Fermi energy of a particular structural evolution configuration while $E_f^q[V_2^i(C_\alpha X)]$ and $E_F^q[V_2^i(C_\alpha X)]$ respectively denote the formation energy and Fermi energy of the corresponding CPDV $V_2^i(C_\alpha X)$ ($i = 1$ or 2, $\alpha = \psi$ or φ, and $X = B$ or N). For the case of $V_2^1(C_\psi N)$, we can note from Fig. 5a that *B* doping and simultaneous healing of graphene is energetically preferred when the system is doped with the charge state being $q \geq -1$ or $q < -3$ while the evolution towards $N_C + \mathrm{DV}_C$ is preferred otherwise. Meanwhile for the case of $V_2^1(C_\varphi B)$ (cf. Fig. 5d), *N* doping and simultaneous healing of graphene is preferred when the system is negatively charged with $q < -1$ while the evolution towards $B_C + \mathrm{DV}_C$ is preferred otherwise.

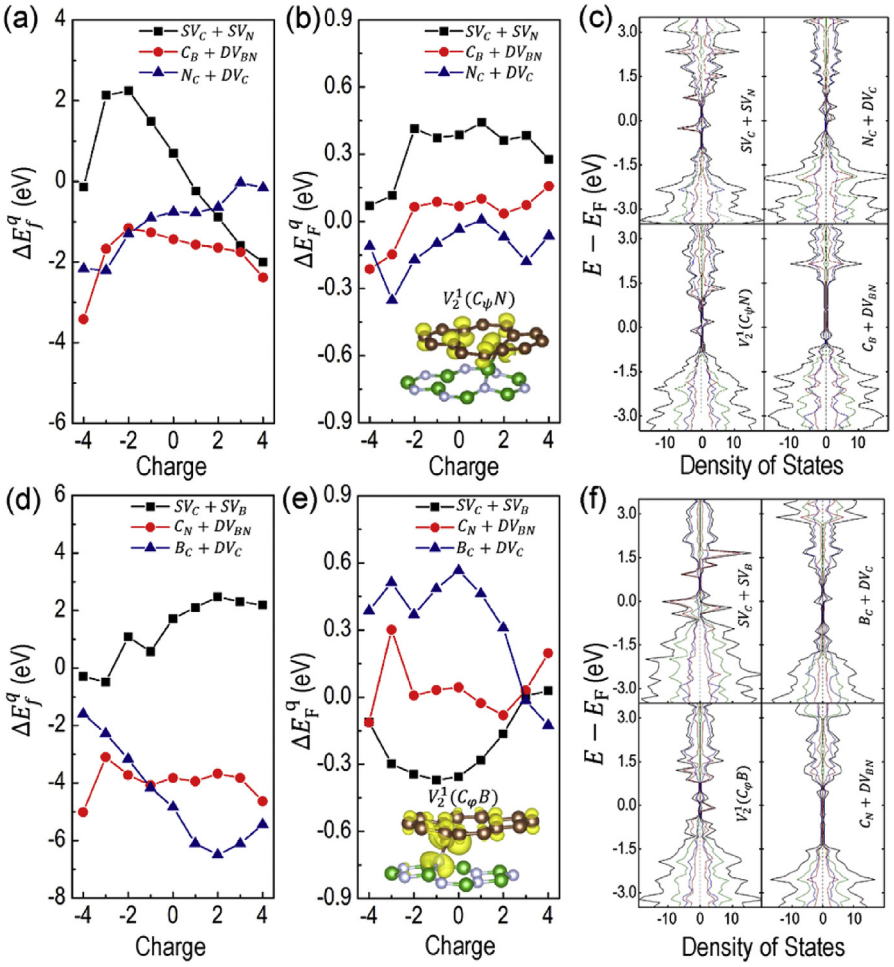

Fig. 5. (a) The formation energy difference ΔE_f^q (cf. Eq. (3)) and (b) Fermi energy difference ΔE_F^q (cf. Eq. (4)) of different structural evolution possibilities at $V_2^1(C_\psi N)$ as functions of the charge state q. (d) ΔE_f^q and (e) ΔE_F^q of different structural evolution possibilities at $V_2^1(C_\varphi B)$. Also shown are the projected density of states (PDOS) plotted for different defect complexes associated with (c) $V_2^1(C_\psi N)$ and (f) $V_2^1(C_\varphi B)$ respectively, with black, green, blue and red lines indicating the total density of states, PDOS from graphene, PDOS from *h*-BN and PDOS contributed by the corresponding impurity states. The insert figures in (b) and (e) illustrate the partial charge of $V_2^1(C_\psi N)$ and $V_2^1(C_\varphi B)$ only contributed by impurity states respectively (A colour version of this figure can be viewed online).

Noting from Eq. (2) that the defect formation energy has an apparent dependence on the Fermi energy E_F^q, and combining Eqs (2)–(4), we have

$$\Delta E_f^q = -q\Delta E_F^q + \left(E_{tot}^q[TS] - E_{tot}^q\left[V_2^i(C_\alpha X)\right]\right), \quad (5)$$

which further yields (denoting $\Delta E_{tot}^q = E_{tot}^q[TS] - E_{tot}^q[V_2^i(C_\alpha X)]$ for simplicity)

$$\frac{\Delta E_f^q}{\partial q} = -\Delta E_F^q + \frac{\partial \Delta E_{tot}^q}{\partial q}, \quad (6)$$

Eq. (6) demonstrates that the variation of ΔE_f^q with respect to q explicitly depends on ΔE_F^q (albeit the presence of $\partial \Delta E_{tot}^q/\partial q$), which is also clearly evident from Fig. 5 (see Supplementary Material for details).

Meanwhile the projected density of states (PDOS) for different defect complexes associated with $V_2^1(C_\psi N)$ and $V_2^1(C_\varphi B)$ are also plotted in Fig. 5 (also see Supplementary Material for corresponding band structures). With the PDOS contributions from graphene, *h*-BN and defect impurity states individually indicated, it shows that the formation difference between ΔE_f^q of different defect complexes mainly come from the impurity states. For those possible defect complexes evolving from CPDVs, we can view them as collections of in-plane defect constituents (i.e., single or di-vacancies, substitutional impurities). Accordingly the Fermi level and band alignment near Fermi level [5,18,60,61] is determined by the characteristics and interplay between the defect constituents involved [35,36,40,42,62–68]. For instance, the Fermi energy generally can be elevated in the presence of *n*-type impurities, e.g., SV_N [35,36,62], but decrease in the presence of *p*-type impurities, e.g., SV_B [36,62,64]. The dependence of the Fermi energy on the defect constituents thus differs with the introduction of charge, as the injected electrons or holes will occupy different energy states (see Supplementary Material for details).

4. Conclusion

In summary, we examined the cross-planar di-vacancies (CPDVs) at graphene/*h*-BN interface. Those extended defects consist of interlayer covalent bonds that act as effective paths for atom diffusion between adjacent graphene and *h*-BN sheets. When directed towards graphene, the CPDV-assisted cross-planar migration induces B or N doping and simultaneous removal of vacancies to heal the lattice structure of graphene. We showed that, by tuning the chemical environment and charge state, the chemical nature of the interlayer bond and associated cross-planar migration pathways at CPDVs can be manipulated to predictively grant consistent B or N doping and healing of graphene. Our findings suggest a viable experimental recipe, combining irradiation, chemical and charge engineering, to produce high-quality graphene with tunable electronic and electrochemical properties, using the *h*-BN substrate.

Acknowledgments

The authors greatly thank the financial support from McGill Engineering Doctorate Award, and NSERC Discovery grant (grant # RGPIN 418469-2012). The authors thank Professor Zetian Mi and Mr Xianhe Liu in the Department of Electrical and Computer Engineering at McGill University for helpful discussion and experimental insights. The authors also would like to acknowledge Supercomputer Consortium Laval UQAM McGill and Eastern Quebec for providing computing power.

Appendix A. Supplementary data

Supplementary data related to this article can be found at http://dx.doi.org/10.1016/j.carbon.2015.10.100.

References

[1] M. Yankowitz, J. Xue, D. Cormode, J.D. Sanchez-Yamagishi, K. Watanabe, T. Taniguchi, et al., Emergence of superlattice dirac points in graphene on hexagonal boron nitride, Nat. Phys. 8 (5) (2012) 382–386.
[2] J.C.W. Song, A.V. Shytov, L.S. Levitov, Electron interactions and gap opening in graphene superlattices, Phys. Rev. Lett. 111 (26) (2013) 266801.
[3] R.V. Gorbachev, J.C.W. Song, G.L. Yu, A.V. Kretinin, F. Withers, Y. Cao, et al., Detecting topological currents in graphene superlattices, Science 346 (6208) (2014) 448–451.
[4] B. Hunt, J.D. Sanchez-Yamagishi, A.F. Young, M. Yankowitz, B.J. LeRoy, K. Watanabe, et al., Massive dirac fermions and hofstadter butterfly in a van der waals heterostructure, Science 340 (6139) (2013) 1427–1430.
[5] J.C.W. Song, P. Samutpraphoot, L.S. Levitov, Topological Bands in G/h-bn Heterostructures, ArXiv e-prints, 2014, p. 4019.
[6] C.R. Woods, L. Britnell, A. Eckmann, R.S. Ma, J.C. Lu, H.M. Guo, et al., Commensurate-incommensurate transition in graphene on hexagonal boron nitride, Nat. Phys. 10 (6) (2014) 451–456.
[7] J. Xue, J. Sanchez-Yamagishi, D. Bulmash, P. Jacquod, A. Deshpande, K. Watanabe, et al., Scanning tunnelling microscopy and spectroscopy of ultra-flat graphene on hexagonal boron nitride, Nat. Mater. 10 (4) (2011) 282–285.
[8] L.A. Ponomarenko, R.V. Gorbachev, G.L. Yu, D.C. Elias, R. Jalil, A.A. Patel, et al., Cloning of dirac fermions in graphene superlattices, Nature 497 (7451) (2013) 594–597.
[9] C.R. Dean, L. Wang, P. Maher, C. Forsythe, F. Ghahari, Y. Gao, et al., Hofstadter's butterfly and the fractal quantum Hall effect in moire superlattices, Nature 497 (7451) (2013) 598–602.
[10] R.H. Telling, C.P. Ewels, A.A. El-Barbary, M.I. Heggie, Wigner defects bridge the graphite gap, Nat. Mater 2 (5) (2003) 333–337.
[11] B. Florian, Irradiation effects in carbon nanostructures, Rep. Prog. Phys. 62 (8) (1999) 1181.
[12] B. Peng, M. Locascio, P. Zapol, S. Li, S.L. Mielke, G.C. Schatz, et al., Measurements of near-ultimate strength for multiwalled carbon nanotubes and irradiation-induced crosslinking improvements, Nat. Nano 3 (10) (2008) 626–631.
[13] C.P. Ewels, R.H. Telling, A.A. El-Barbary, M.I. Heggie, P.R. Briddon, Metastable frenkel pair defect in graphite: source of wigner energy? Phys. Rev. Lett. 91 (2) (2003) 025505.
[14] A.J.R. da Silva, A. Fazzio, A. Antonelli, Bundling up carbon nanotubes through wigner defects, Nano Lett. 5 (6) (2005) 1045–1049.
[15] A. Kis, G. Csanyi, J.P. Salvetat, T.-N. Lee, E. Couteau, A.J. Kulik, et al., Reinforcement of single-walled carbon nanotube bundles by intertube bridging, Nat. Mater. 3 (3) (2004) 153–157.
[16] J. Song, B. Ouyang, N.V. Medhekar, Energetics and kinetics of li intercalation in irradiated graphene scaffolds, ACS Appl. Mater. Interfaces 5 (24) (2013) 12968–12974.
[17] K. Sengupta, G. Baskaran, Tuning Kondo physics in graphene with gate voltage, Phys. Rev. B 77 (4) (2008) 045417.
[18] G. Giovannetti, P.A. Khomyakov, G. Brocks, P.J. Kelly, J. van den Brink, Substrate-induced band gap in graphene on hexagonal boron nitride: ab initio desity funtional caculations, Phys. Rev. B 76 (7) (2007) 073103.
[19] H. Nematian, M. Moradinasab, M. Pourfath, M. Fathipour, H. Kosina, Optical properties of armchair graphene nanoribbons embedded in hexagonal boron nitride lattices, J. Appl. Phys. 111 (9) (2012) 093512.
[20] G. Kresse, J. Furthmüller, Efficient iterative schemes for ab initio total energy calculations using a plane-wave basis set, Phys. Rev. B 54 (16) (1996) 11169–11186.
[21] P.E. Blöchl, Projector augmented-wave method, Phys. Rev. B 50 (24) (1994) 17953–17979.
[22] P. Hohenberg, W. Kohn, Inhomogeneous electron gas, Phys. Rev. 136 (3B) (1964) B864–B871.
[23] W. Kohn, L.J. Sham, Self-consistent equations including exchange and correlation effects, Phys. Rev. 140 (4A) (1965) A1133–A1138.
[24] J.P. Perdew, K. Burke, M. Ernzerhof, Generalized gradient approximation made simple, Phys. Rev. Lett. 77 (18) (1996) 3865–3868.
[25] D. Sheppard, P. Xiao, W. Chemelewski, D.D. Johnson, G. Henkelman, A generalized solid-state nudged elastic band method, J. Chem. Phys. 136 (7) (2012) 074103.
[26] D. Sheppard, R. Terrell, G. Henkelman, Optimization methods for finding minimum energy paths, J. Chem. Phys. 128 (13) (2008) 134106.
[27] G. Henkelman, B.P. Uberuaga, H. Jónsson, A climbing image nudged elastic band method for finding saddle points and minimum energy paths, J. Chem. Phys. 113 (22) (2000) 9901–9904.
[28] R.A. Olsen, G.J. Kroes, G. Henkelman, A. Arnaldsson, H. Jónsson, Comparison of methods for finding saddle points without knowledge of the final states, J. Chem. Phys. 121 (20) (2004) 9776–9792.
[29] S. Grimme, Semiempirical GGA-type density functional constructed with a long-range dispersion correction, J. Comput. Chem. 27 (15) (2006)

1787–1799.
[30] T. Kuila, S. Bose, A.K. Mishra, P. Khanra, N.H. Kim, J.H. Lee, Chemical functionalization of graphene and its applications, Prog. Mater. Sci. 57 (7) (2012) 1061–1105.
[31] D. Vanpoucke, G. Brocks, Formation of Pt-induced Ge atomic nanowires on Pt/Ge(001): a density functional theory study, Phys. Rev. B 77 (24) (2008) 241308.
[32] D.E.P. Vanpoucke, Ab Initio Study of Pt Induced Nanowires on Ge(001), 2009.
[33] F. Banhart, J. Kotakoski, A.V. Krasheninnikov, Structural defects in graphene, ACS Nano 5 (1) (2010) 26–41.
[34] Y.-F. Lu, S.-T. Lo, J.-C. Lin, W. Zhang, J.-Y. Lu, F.-H. Liu, et al., Nitrogen-doped graphene sheets grown by chemical vapor deposition: synthesis and influence of nitrogen impurities on carrier transport, ACS Nano 7 (8) (2013) 6522–6532.
[35] N. Berseneva, A. Krasheninnikov, R. Nieminen, Mechanisms of postsynthesis doping of boron nitride nanostructures with carbon from first-principles simulations, Phys. Rev. Lett. 107 (3) (2011) 035501.
[36] B. Huang, H. Lee, Defect and impurity properties of hexagonal boron nitride: a first-principles calculation, Phys. Rev. B 86 (24) (2012) 245406.
[37] A. Zobelli, C. Ewels, A. Gloter, G. Seifert, Vacancy migration in hexagonal boron nitride, Phys. Rev. B 75 (9) (2007) 094104.
[38] P. Rani, V.K. Jindal, Designing band gap of graphene by B and N dopant atoms, RSC Adv. 3 (3) (2013) 802–812.
[39] Y. Kim, J. Ihm, E. Yoon, G.-D. Lee, Dynamics and stability of divacancy defects in graphene, Phys. Rev. B 84 (7) (2011) 075445.
[40] M.M. Ugeda, I. Brihuega, F. Hiebel, P. Mallet, J.-Y. Veuillen, J.M. Gómez-Rodríguez, et al., Electronic and structural characterization of divacancies in irradiated graphene, Phys. Rev. B 85 (12) (2012) 121402.
[41] Z.-H. Sheng, H.-L. Gao, W.-J. Bao, F.-B. Wang, X.-H. Xia, Synthesis of boron doped graphene for oxygen reduction reaction in fuel cells, J. Mater. Chem. 22 (2) (2012) 390–395.
[42] H. Wang, T. Maiyalagan, X. Wang, Review on recent progress in nitrogen-doped graphene: synthesis, characterization, and its potential applications, ACS Catal. 2 (5) (2012) 781–794.
[43] R. Lv, Q. Li, A.R. Botello-Méndez, T. Hayashi, B. Wang, A. Berkdemir, et al., Nitrogen-doped graphene: beyond single substitution and enhanced molecular sensing, Sci. Rep. 2 (586) (2012) 1–8.
[44] V. Georgakilas, M. Otyepka, A.B. Bourlinos, V. Chandra, N. Kim, K.C. Kemp, et al., Functionalization of graphene: covalent and non-covalent approaches, derivatives and applications, Chem. Rev. 112 (11) (2012) 6156–6214.
[45] P.M. Ajayan, V. Ravikumar, J.C. Charlier, Surface reconstructions and dimensional changes in single-walled carbon nanotubes, Phys. Rev. Lett. 81 (7) (1998) 1437–1440.
[46] M. Terrones, H. Terrones, F. Banhart, J.-C. Charlier, P.M. Ajayan, Coalescence of single-walled carbon nanotubes, Science 288 (5469) (2000) 1226–1229.
[47] M. Terrones, F. Banhart, N. Grobert, J.C. Charlier, H. Terrones, P.M. Ajayan, Molecular junctions by joining single-walled carbon nanotubes, Phys. Rev. Lett. 89 (7) (2002) 075505.
[48] H. Stahl, J. Appenzeller, R. Martel, P. Avouris, B. Lengeler, Intertube coupling in ropes of single-wall carbon nanotubes, Phys. Rev. Lett. 85 (24) (2000) 5186–5189.
[49] A.V. Krasheninnikov, K. Nordlund, M. Sirviö, E. Salonen, J. Keinonen, Formation of ion-irradiation-induced aomic-scale defects on walls of carbon nanotubes, Phys. Rev. B 63 (24) (2001) 245405.
[50] H.-P. Komsa, J. Kotakoski, S. Kurasch, O. Lehtinen, U. Kaiser, A.V. Krasheninnikov, Two-dimensional transition metal dichalcogenides under electron irradiation: defect production and doping, Phys. Rev. Lett. 109 (3) (2012) 035503.
[51] H.-P. Komsa, S. Kurasch, O. Lehtinen, U. Kaiser, A.V. Krasheninnikov, From point to extended defects in two-dimensional MoS2: evolution of atomic structure under electron irradiation, Phys. Rev. B 88 (3) (2013) 035301.
[52] T.-Y. Kim, K. Cho, W. Park, J. Park, Y. Song, S. Hong, et al., Irradiation effects of high-energy proton beams on MoS2 field effect transistors, ACS Nano 8 (3) (2014) 2774–2781.
[53] O.L. Krivanek, M.F. Chisholm, V. Nicolosi, T.J. Pennycook, G.J. Corbin, N. Dellby, et al., Atom-by-atom structural and chemical analysis by annular dark-field electron microscopy, Nature 464 (7288) (2010) 571–574.
[54] A. Zobelli, A. Gloter, C.P. Ewels, G. Seifert, C. Colliex, Electron knock-on cross section of carbon and boron nitride nanotubes, Phys. Rev. B 75 (24) (2007) 245402.
[55] H.-P. Komsa, N. Berseneva, A.V. Krasheninnikov, R.M. Nieminen, Charged point defects in the flatland: accurate formation energy calculations in two-dimensional materials, Phys. Rev. X 4 (3) (2014) 031044.
[56] C. Freysoldt, B. Grabowski, T. Hickel, J. Neugebauer, G. Kresse, A. Janotti, et al., First-principles calculations for point defects in solids, Rev. Mod. Phys. 86 (1) (2014) 253–305.
[57] D.K. Efetov, P. Kim, Controlling electron-phonon interactions in graphene at ultrahigh carrier densities, Phys. Rev. Lett. 105 (25) (2010) 256805.
[58] A.V. Shytov, M.I. Katsnelson, L.S. Levitov, Vacuum polarization and screening of supercritical impurities in graphene, Phys. Rev. Lett. 99 (23) (2007) 236801.
[59] O.V. Yazyev, A. Pasquarello, Effect of metal elements in catalytic growth of carbon nanotubes, Phys. Rev. Lett. 100 (15) (2008) 156102.
[60] J. Sławińska, I. Zasada, Z. Klusek, Energy gap tuning in graphene on hexagonal boron nitride bilayer system, Phys. Rev. B 81 (15) (2010) 155433.
[61] K.-T. Lam, Y. Lu, Y.P. Feng, G. Liang, Stability and electronic structure of two dimensional Cx(BN)y compound, Appl. Phys. Lett. 98 (2) (2011).
[62] B. Ouyang, J. Song, Strain engineering of magnetic states of vacancy-decorated hexagonal boron nitride, Appl. Phys. Lett. 103 (10) (2013) 102401.
[63] L. Wang, Z. Sofer, P. Šimek, I. Tomandl, M. Pumera, Boron-doped graphene: scalable and tunable p-type carrier concentration doping, J. Phys. Chem. C 117 (44) (2013) 23251–23257.
[64] B. Huang, H. Xiang, J. Yu, S.-H. Wei, Effective control of the charge and magnetic states of transition-metal atoms on single-layer boron nitride, Phys. Rev. Lett. 108 (20) (2012) 206802.
[65] B. Huang, S.-H. Wei, Comment on mechanisms of postsynthesis doping of boron nitride nanostructures with carbon from first-principles simulations', Phys. Rev. Lett. 107 (23) (2011) 239601.
[66] N. Berseneva, A.V. Krasheninnikov, R.M. Nieminen, Berseneva, krasheninnikov, and nieminen reply, Phys. Rev. Lett. 107 (23) (2011) 239602.
[67] B. Wang, S.T. Pantelides, Magnetic moment of a single vacancy in graphene and semiconducting nanoribbons, Phys. Rev. B 86 (16) (2012) 165438.
[68] J.-J. Chen, H.-C. Wu, D.-P. Yu, Z.-M. Liao, Magnetic moments in graphene with vacancies, Nanoscale 6 (15) (2014) 8814–8821.